Plant Biotechnology Journal
Open Access

Plant Biotechnology Journal (2021) **19**, pp. 977–991 doi: 10.1111/pbi.13523

Citrus miraculin-like protein hijacks a viral movement-related p33 protein and induces cellular oxidative stress in defence against *Citrus tristeza virus*

Yong-Duo Sun[1,2,*], Lei Zhang[1,a] and Svetlana Y. Folimonova[1,2,*]

[1]*Department of Plant Pathology, University of Florida, Gainesville, FL, USA*
[2]*Plant Molecular and Cellular Biology Program, University of Florida, Gainesville, FL, USA*

Received 29 April 2020;
revised 26 October 2020;
accepted 30 November 2020.
*Correspondence (Tel +1 (352) 871 4715; fax (352) 392 6532; email yd.sun@ufl.edu (Y.D.S.), Tel +1 (352) 273 4655; fax (352) 392 6532; email svetlana@ufl.edu (S.Y.F.))
[a]Present address: College of Horticulture and Plant Protection, Inner Mongolia Agricultural University, Hohhot, 010018, China

Keywords: *Citrus tristeza virus*, miraculin-like protein, p33 protein, virus movement, cellular oxidative stress.

Summary

To defend against pathogens, plants have developed a complex immune system, which recognizes the pathogen effectors and mounts defence responses. In this study, the p33 protein of *Citrus tristeza virus* (CTV), a viral membrane-associated effector, was used as a molecular bait to explore virus interactions with host immunity. We discovered that *Citrus macrophylla* miraculin-like protein 2 (CmMLP2), a member of the soybean Kunitz-type trypsin inhibitor family, targets the viral p33 protein. The expression of *CmMLP2* was up-regulated by p33 in the citrus phloem-associated cells. Knock-down of the *MLP2* expression in citrus plants resulted in a higher virus accumulation, while the overexpression of *CmMLP2* reduced the infectivity of CTV in the plant hosts. Further investigation revealed that, on the one hand, binding of CmMLP2 interrupts the cellular distribution of p33 whose proper function is necessary for the effective virus movement throughout the host. On the other hand, the ability of CmMLP2 to reorganize the endomembrane system, amalgamating the endoplasmic reticulum and the Golgi apparatus, induces cellular stress and accumulation of the reactive oxygen species, which inhibits the replication of CTV. Altogether, our data suggest that CmMLP2 employs a two-way strategy in defence against CTV infection.

Introduction

In many parts of the world, production of citrus, one of the most economically important fruit crops, is severely impacted by *Citrus tristeza virus* (CTV)-induced diseases. CTV, which belongs to the family *Closteroviridae*, infects phloem-associated cells of *Citrus* spp. and citrus relatives. Citrus trees affected by CTV show a range of syndromes, including quick decline and death of trees grafted on the sour orange rootstock and stem pitting that is accompanied by the abnormal vascular development and production of small non-marketable fruits. During the last century, CTV killed millions of citrus trees and severely reduced the yield of citrus worldwide (Dawson *et al.*, 2015; Moreno *et al.*, 2008). The ultimate means to control CTV diseases are still lacking. One of the strategies to protect citrus from CTV infection is planting resistant citrus cultivars that are generated through molecular breeding. Our understanding of the plant host–CTV interactions, however, is limited, especially, that of the molecular basis of the host defence components involved in response to the virus infection (Dawson *et al.*, 2013). Thus, exploration of the molecular mechanisms mediating citrus host defence against CTV and identification of the corresponding resistance genes, which will provide necessary information for generating CTV-resistant citrus species, is urgent.

In the arms race between plants and their pathogens, plant hosts have developed a multi-level defence system to limit or even block pathogen infection. The concepts of the classical zigzag model of plant immunity (Jones and Dangl, 2006) have been recently integrated into plant–virus interactions. Two major mechanisms are implicated in plant response to virus infection: RNA silencing and resistance (R) gene-mediated defence. Viral double-stranded RNA is viewed as a pathogen-associated molecular pattern (PAMP) analog, and RNA silencing-based host defence is considered as a form of a PAMP-triggered immunity response. Certain viral proteins serve as effectors, which interact with the specific R proteins leading to viral effector-triggered immunity. In many instances, viral proteins such as coat proteins, movement proteins, and those that suppress RNA silencing were found to function as viral effectors. In addition to the R proteins, other host proteins have been shown to confer the host resistance against diverse viral infections, including certain translation initiation factors, endoplasmic reticulum (ER)-residing chaperones and lectin proteins (Liu *et al.*, 2017; Mandadi and Scholthof, 2013; Zvereva and Pooggin, 2012). Often, various pathways undergo crosstalk and maximize the downstream responses such as a hypersensitive response/necrotic response, reactive oxygen species (ROS) burst and the expression of plant immunity-associated genes to defeat virus invasion.

The CTV genome is *ca.* 19.3 kb and is organized into 12 open reading frames (ORFs). ORFs 1a and 1b are expressed directly from the 5′ half of the genomic RNA and encode polyproteins, which are required for virus replication. The ORFs

2-11 are translated through 3′-coterminal subgenomic RNAs. The corresponding proteins—p33, p6, p65 (a 70-kDa heat-shock protein homolog/HSP70h), p61, minor coat protein (CPm), coat protein (Cp), p18, p13, p20 and p23—were shown to function at different stages of the virus infection cycle (Dolja *et al*., 2006; Folimonova, 2012; Karasev *et al*., 1995; Lu *et al*., 2004; Tatineni *et al*., 2011). Recently, we demonstrated that, among the CTV-encoded proteins, p20, p23 and p33 could trigger host immune responses such as ROS accumulation and programmed cell death (PCD) in *Nicotiana benthamiana*. Furthermore, we found that the p33 protein plays a role of a viral effector, which influences the virus pathogenicity by modulating a host immune response (Sun and Folimonova, 2019). Yet, how host immunity recognizes the p33 protein and mediates the downstream responses remained unexplored. In this work, we used p33 as a molecular bait and discovered that citrus miraculin-like protein 2 (MLP2), a member of the soybean Kunitz-type trypsin inhibitor (KTI) super-family, could interact with the p33 protein. Interestingly, earlier transcriptomic and proteomic analyses have shown that the citrus MLP2 could be induced by CTV but the role of MLP2 during CTV infection and the underlying mechanism remained unknown (Dória *et al*., 2015; Gandía *et al*., 2007). Here, we bring multiple evidence that citrus MLP2 has a dual function in host defence against CTV infection: MLP2 hijacks the p33 protein, which results in the impediment of the viral systemic spread, and simultaneously induces cellular oxidative stress that suppresses virus replication in the host.

Results

The N-terminal portion of p33 that lacks the protein transmembrane domain is responsible for the induction of ROS accumulation in the host plants

The p33 protein contains a 22-amino acid-long transmembrane domain (TMD) at the C-terminal end (Fig. S1A; Kang *et al*., 2015). To assess whether TMD is required for the p33-mediated induction of the host immune responses in the plant hosts, a green fluorescent protein-tagged TMD (GFP-TMD) and a GFP-tagged N-terminal portion of p33 lacking TMD (GFP-p33ΔTMD) were transiently expressed in *N. benthamiana* by *Agrobacterium tumefaciens*-mediated transformation, along with a full-length non-tagged p33 and a GFP-tagged p33 (GFP-p33) as the positive controls (Fig. S1A). Examination of the infiltrated leaf patches at 14 days post-infiltration (dpi) showed that ectopic expression of the full-length p33 and GFP-p33 caused visible necrosis, and expression of GFP-p33ΔTMD resulted in a chlorotic phenotype. In contrast, no cell death or chlorosis was observed upon GFP-TMD expression (Fig. S1B). The plant leaves were further subjected to 3,3′-diaminobenzidine (DAB) staining, which detects the most abundant component of ROS —hydrogen peroxide. DAB staining revealed the development of a strong dark brown colour in the necrotic leaf patches expressing p33 and GFP-p33 and an attenuated brown colour in the leaf patch expressing GFP-p33ΔTMD, indicating a high concentration of ROS accumulation. Only a pale yellowish colour was observed in the leaf patch expressing GFP-TMD (Fig. S1C). Collectively, these data suggested that p33ΔTMD is responsible for triggering ROS in the plant hosts, while the C-terminal TMD appears to influence the intensity of such host immune responses.

CmMLP2 interacts with the p33 protein of CTV *in vivo*

To dissect the underlying mechanism of how plant immunity recognizes the p33 protein, a yeast two-hybrid (Y2H) assay was employed to identify a candidate protein(s) in citrus that interacts with p33. By conducting a Y2H screening and a pairwise Y2H assay, a *C. macrophylla* homolog of *Citrus cv*. Shiranuhi putative MLP2 (Genbank accession EF122397.1) was shown to interact with the p33ΔTMD (Figure 1a). Hereafter, we refer to the selected gene as *C. macrophylla miraculin-like protein 2* (*CmMLP2*) gene (Genbank accession MT310721). At the next step, a co-immunoprecipitation (Co-IP) assay was used to verify that CmMLP2 could interact with the full-length p33. As shown in Figure 1b, a red fluorescent protein-tagged p33 (RFP-p33) could co-immunoprecipitate with a mGFP-tagged CmMLP2 (CmMLP2-mGFP), but not with the control free mGFP. Confocal microscopy examination of the subcellular distribution of p33 and CmMLP2 tagged with the fluorescent proteins revealed that the two proteins localized to the same cellular compartments in the epidermal cells of *N. benthamiana* (Figure 1c). Altogether, these assays confirmed that CmMLP2 could interact with p33 *in vivo*.

The *CmMLP2* expression in the phloem-associated cells is induced in response to p33

MLPs share high sequence similarity with miraculin and are classified into the KTI family as they share a Kunitz motif that could inhibit serine, cysteine, and aspartic acid proteases (Brouwer *et al*., 1968; Selvakumar *et al*., 2011; Takai *et al*., 2013). It has been reported that expression of citrus *MLP2* could be induced by CTV infection in the sweet orange variety Westin' (*C. sinensis* (L.) Osbeck) (Dória *et al*., 2015). Multiple sequence alignments indicated that MLP2 homologs are highly conserved in citrus varieties, including *C. sinensis* and *C. macrophylla* (Fig. S2). Reverse transcription-quantitative PCR (RT-qPCR) showed that the CTV-infected young branches of 2-year-old *C. macrophylla* seedlings had a higher level of the *CmMLP2* expression, compared to that of the healthy control (Figure 1d). Since CmMLP2 interacts with the p33 protein of CTV *in vivo*, we next tested whether p33 is one of the viral factors that account for the up-regulation of *CmMLP2*. By analysing the transcript level of *CmMLP2* in the citrus seedlings that were infected with a CTV mutant lacking the *p33* gene (CTV:Δp33), we found that the CTV:Δp33 mutant cannot induce *CmMLP2* expression at three months post-inoculation (mpi) in the young stems of *C. macrophylla*: the expression level of *CmMLP2* in those plants was almost identical to that of the healthy control (Figure 1d). These results indicated that p33 is necessary to induce citrus *MLP2* accumulation during CTV infection in the young citrus flushes.

Furthermore, to determine whether the p33 protein itself is sufficient to induce the *CmMLP2* expression, three independent p33-overexpressing transgenic *C. macrophylla* lines referred to as OEp33-1, OEp33-3 and OEp33-4 were generated. Compared to the wild-type control, the transgenic lines showed high levels of the p33 expression as was detected by RT-PCR using the *p33*-specific oligonucleotides and Western blotting with a p33-specific antibody (Fig. S3A, B, C). The RT-qPCR analysis demonstrated that the transcript levels of *CmMLP2* in the three transgenic citrus lines were all increased, compared to the non-transgenic control (about 6-, 3- and 4-folds higher, respectively) (Figure 1e). These data suggested that the expression of the p33 protein is sufficient to up-regulate the expression of *CmMLP2*.

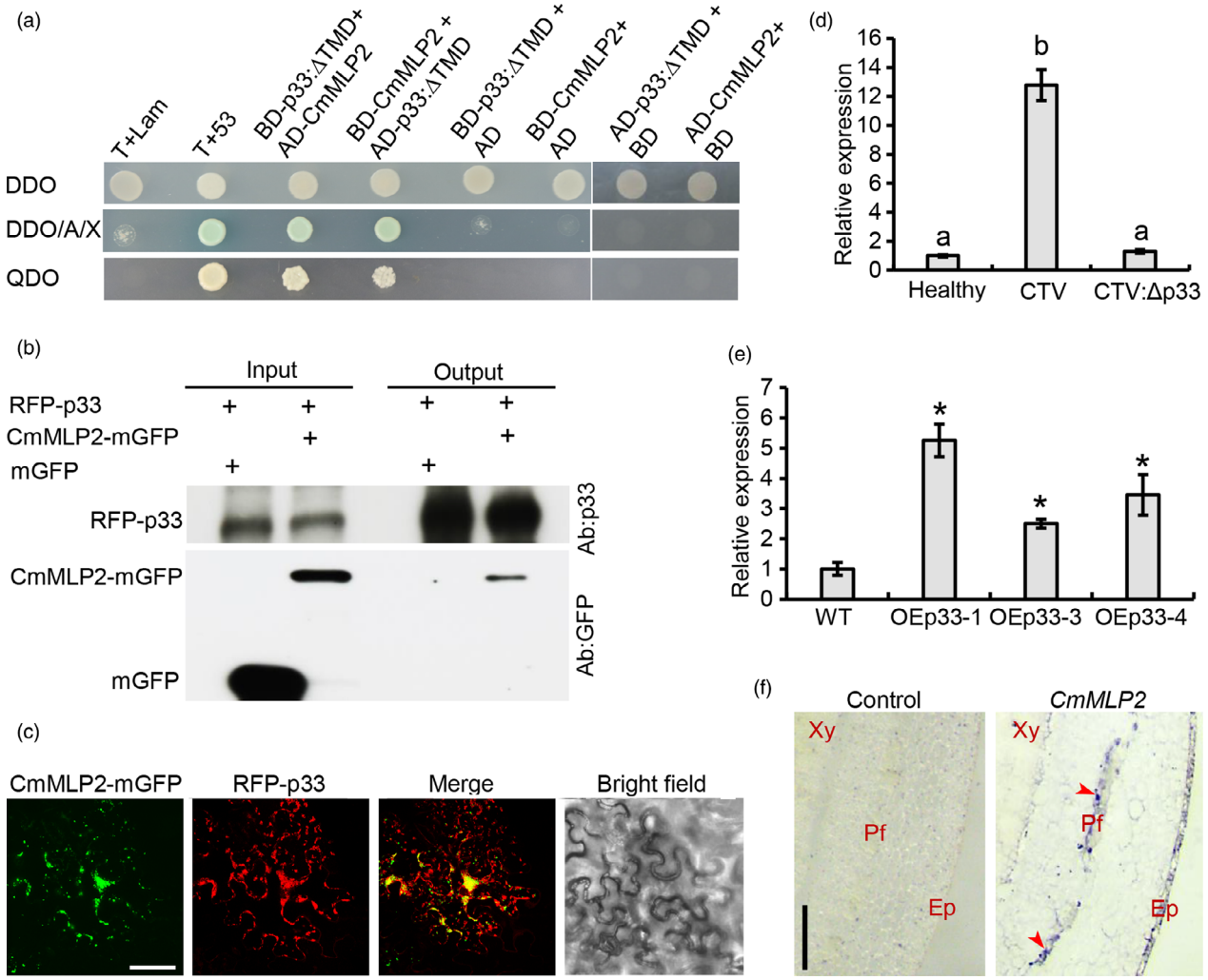

Figure 1 CmMLP2 is associated with the p33 protein of CTV. (a), Yeast two-hybrid-based examination of the interaction between CmMLP2 and the p33 protein lacking its transmembrane domain (p33ΔTMD). Yeast cells transformed with the indicated constructs were grown on SD/-Leu/-Trp DO (DDO) medium, DDO medium plus 200 ng/mL Aureobasidin A and 40 μg/mL X-a-Gal (DDO/X/A), and SD/–Leu/–Trp/–Ade/–His DO (QDO) medium for 72 h at 30°C. (b), Co-immunoprecipitation assay. RFP-p33 was used as a bait, and CmMLP2-GFP was used as a prey. A p33-specific antibody (Ab:p33) was used to detect RFP-p33. The GFP antibody (Ab:GFP) was used to detect free mGFP and CmMLP2-mGFP. (c), Subcellular colocalization of CmMLP2-mGFP and RFP-p33. Yellow fluorescence indicates the colocalization of the two fluorescent protein-tagged partners. Bar = 50 μm. (d), The relative expression of *CmMLP2* in healthy and CTV- or CTV:Δp33-infected citrus. Values represent the mean ± SD (n = 3). Different letters stand for statistically significant differences at $P < 0.05$ (Student's t-test). A similar tendency was obtained from at least three biological repeats. (e), The relative expression of *CmMLP2* in OEp33 transgenic *C. macrophylla* lines. Values represent the mean ± SD (n = 3). The asterisks denote statistically significant differences as determined by Student's t-test (*, $P < 0.05$). (f), Observation of the distribution of *CmMLP2* transcripts in the CTV-infected citrus stem. The distribution of *CmMLP2* was detected by *in situ* hybridization. Left panel: probe-free negative control. Right panel: *in situ* hybridization using antisense-*CmMLP2* probe. Xy: xylem. Pf: phloem fibre. Ep: epidermal cells. Bar = 0.5 mm.

As the level of the *CmMLP2* expression was p33-responsive, we hypothesized that the two proteins share the same spatial niche in citrus. Firstly, we examined the accumulation of the p33 protein during CTV infection using a CTV variant expressing a GFP-tagged p33 (CTV:GFP-p33) (Fig. S4A, Kang *et al.*, 2015). As expected, accumulation of GFP-p33 was visualized in the phloem-associated cells of the CTV:GFP-p33-infected *C. macrophylla* (Fig. S4B). At the next step, an *in situ* hybridization assay was used to examine the distribution of the *CmMLP2* transcripts in the stems of the CTV-infected citrus plants. As shown in Figure 1f, *CmMLP2* had a markedly high expression level in the phloem-associated cells of *C. macrophylla*, which represents a typical niche of the p33 accumulation.

Altogether, these results indicated that CmMLP2 accumulates in response to the p33 expression in the phloem-associated cells during the CTV infection.

CmMLP2 functions in defence against CTV infection

To investigate the function of CmMLP2 in defence against CTV, we first analysed the citrus plants with a decreased CmMLP2 expression. The CTV-based virus-induced gene silencing (VIGS) approach was employed to knock-down the transcript of *CmMLP2* in citrus plants. The ability of CTV to serve as an

efficient VIGS vector for silencing plant genes was shown previously and confirmed here using a CTV variant carrying a fragment of a citrus phytoene desaturase gene (*PDS*; CTV-tPDS) (Fig. S5, Hajeri *et al*., 2014). To silence *CmMLP2*, a sequence corresponding to a truncated *CmMLP2* gene (tMLP2) was introduced at the 3′ terminal end of the CTV genome resulting in a virus variant that we referred to as CTV-tMLP2 (Figure 2a). The transmission electron microscopy (TEM) observations confirmed that insertion of tMLP2 in the CTV genome did not affect formation of virions (Figure 2b). At the next step, the virions of CTV-tMLP2 were inoculated into two-year-old *C. macrophylla* trees using the 'bark-flap' method. The control *C. macrophylla* were inoculated with the wild-type CTV. At three mpi, the RT-qPCR data confirmed that the CTV-tMLP2 virus silenced the expression of *CmMLP2* in the inoculated citrus plants (Figure 2c). Virus quantification by enzyme-linked immunosorbent assay (ELISA) showed that a titre of CTV-tMLP2 in the inoculated plants was higher, compared to that of the wild-type CTV control, though the difference between the titres of the two viruses was not statistically significant (Figure 2d). Considering that the citrus *MLP2* sequences are highly conserved (Fig. S2), sweet orange 'Madame Vinous' (*C. sinensis* (L.) Osbeck), a citrus cultivar that exhibits a decreased susceptibility to CTV, compared to that of *C. macrophylla,* was used as an alternative host. The *C. macrophylla* budwood tissue harbouring CTV-tMLP2 or wild-type CTV was used for graft inoculation into the *C. sinensis* (L.) Osbeck trees. At two mpi, the *C. sinensis* plants inoculated with CTV-tMLP2 showed silencing of the host *MLP2* expression and a much higher virus titre, compared to that upon the wild-type CTV infection (Fig. S6, Figure 2e).

In addition to using the CTV-based VIGS approach to silence *MLP2* upon virus infection, gain-of-function approaches were also employed. Nine independent *CmMLP2*-overexpression transgenic Mexican lime (*C. aurantifolia*) lines were generated, and three of them (OEMLP2:91-2, OEMLP2:91-4, OEMLP2:91-6) were chosen for further examination. The wild-type *C. aurantifolia* trees with low expression of citrus *MLP2* were used as control (Figure 2f). The plants were inoculated with the RFP-tagged CTV variant (CTV-RFP; Atallah *et al*., 2016) using the 'bark-flap' method. At three mpi, as shown in Figure 2g, fewer cells infected with the virus were observed in the *CmMLP2*-overexpression trees, compared to those in the control plants. Virus quantification using ELISA confirmed that the overexpression of *CmMLP2* led to an increase in the citrus resistance to CTV (Figure 2g).

Collectively, these data demonstrated that the expression level of citrus *MLP2* is tightly associated with the resistance of host plants to CTV infection.

CmMLP2 hijacks the p33 protein to form condensed aggregations

Since CmMLP2 is induced by and interacts with the p33 protein of CTV, we hypothesized that CmMLP2 could interfere with a function(s) of p33, which consequently impedes virus infection and, thus, defends a host against CTV. To understand the association between the two proteins, we examined the subcellular distribution of p33 upon CTV infection in the plant hosts using confocal microscopy. In the CTV:GFP-p33-infected *C. macrophylla*, the GFP-p33 localized at the cellular membrane as well formed vesicles in the cytosol of the phloem companion cells (Figure 3a). Similar distribution of the protein was also observed in the epidermal cells of leaves of a viral herbaceous laboratory host *N. benthamiana*, which were infiltrated with the *Agrobacterium* culture (OD_{600} = 0.1) harbouring *pCTV:GFP-p33*, confirming that the cellular membrane deposition and vesicle formation are the characteristic features of the p33 intracellular distribution in virus hosts (Figure 3b). Next, a RFP-tagged CmMLP2 (CmMLP2-RFP) and the free RFP, as a control, were transiently co-expressed with CTV:GFP-p33 in *N. benthamiana* through agroinfiltration. As shown in Figure 3c, the free RFP had no effect on the cellular distribution of p33 at seven dpi: p33 still localized at the cellular membrane and formed intracellular vesicles. However, the introduction of CmMLP2-RFP dramatically changed the distribution of p33: CmMLP2-RFP and GFP-p33 colocalized in the large dense aggregations within the cell.

Altogether, these data indicated that CmMLP2 could hijack p33 and alter its subcellular distribution.

The p33 protein plays a role in the CTV systemic spread

In the previous studies, membrane localization of p33 was suggested to be associated with its role in virus translocation (Bak and Folimonova, 2015). To address the biological significance of the p33 protein being hijacked by CmMLP2 in a host response to CTV invasion, we further assessed the role of the p33 protein in virus movement. The spread of the GFP-tagged wild-type CTV (CTV-GFP) and CTV:Δp33 (CTV-GFP:Δp33) were compared in the *N. benthamiana* plants. Three whole leaves of the *N. benthamiana* plants were infiltrated with the *Agrobacterium* cultures (OD_{600} = 0.1), each harbouring *pCTV-GFP*, *pCTV-GFP:Δp33*, or the empty vector, respectively. As shown in Figure 4a (upper panel), at one-week post-infiltration (wpi), no GFP signal was observed in the lower leaves infiltrated with *Agrobacterium* harbouring the empty vector, whereas leaves infiltrated with the cultures containing either *pCTV-GFP* or *pCTV-GFP:Δp33* showed strong GFP production. With that, the level of GFP was higher in the leaves expressing CTV-GFP:Δp33, compared with that upon CTV-GFP expression, indicating higher virus accumulation in the case of the p33 deletion mutant, which correlated with the observations made in our earlier work (Sun and Folimonova, 2019). At four wpi, the CTV-GFP-infected plants showed a marked spread of the GFP signal at both the aboveground (stem and upper leaves) and underground (roots) levels. However, only scattered GFP signal was seen in the distal parts of the CTV-GFP:Δp33-infected plants, which indicated that the speed and the efficiency of the wild-type CTV systemic spread was higher than that of CTV-GFP:Δp33 (Figure 4a, lower panel). The difference in the titres of the two virus variants in the upper leaves of the *N. benthamiana* plants was also confirmed by virus quantification through semi-quantitative RT-PCR using the CTV-specific primers (Figure 4b). These observations indicated that, in *N. benthamiana*, p33 affects the efficiency of the virus systemic spread.

Furthermore, we compared the speed of the two CTV variants translocation in *C. macrophylla*, by setting up a 'virus-racing' assay (Figure 4c). The virions of the two variants were extracted from the leaves of the *N. benthamiana* plants, and the virus titre was tested prior to inoculation to ensure a similar amount of the virus inoculum was used in each treatment (Fig. S7). The tissue collection site on the inoculated *C. macrophylla* trees was set at approximately 50 cm above the inoculation site. As shown in Figure 4d, at three mpi, examination of the plant tissue for the GFP expression coupled with the ELISA analysis showed that 100% of the citrus plants inoculated with CTV-GFP established a successful infection. At this time point, only 20% of the CTV-GFP:Δp33-inoculated plants showed infection in the upper stem. The virus lacking p33 had an apparent delay in the development of

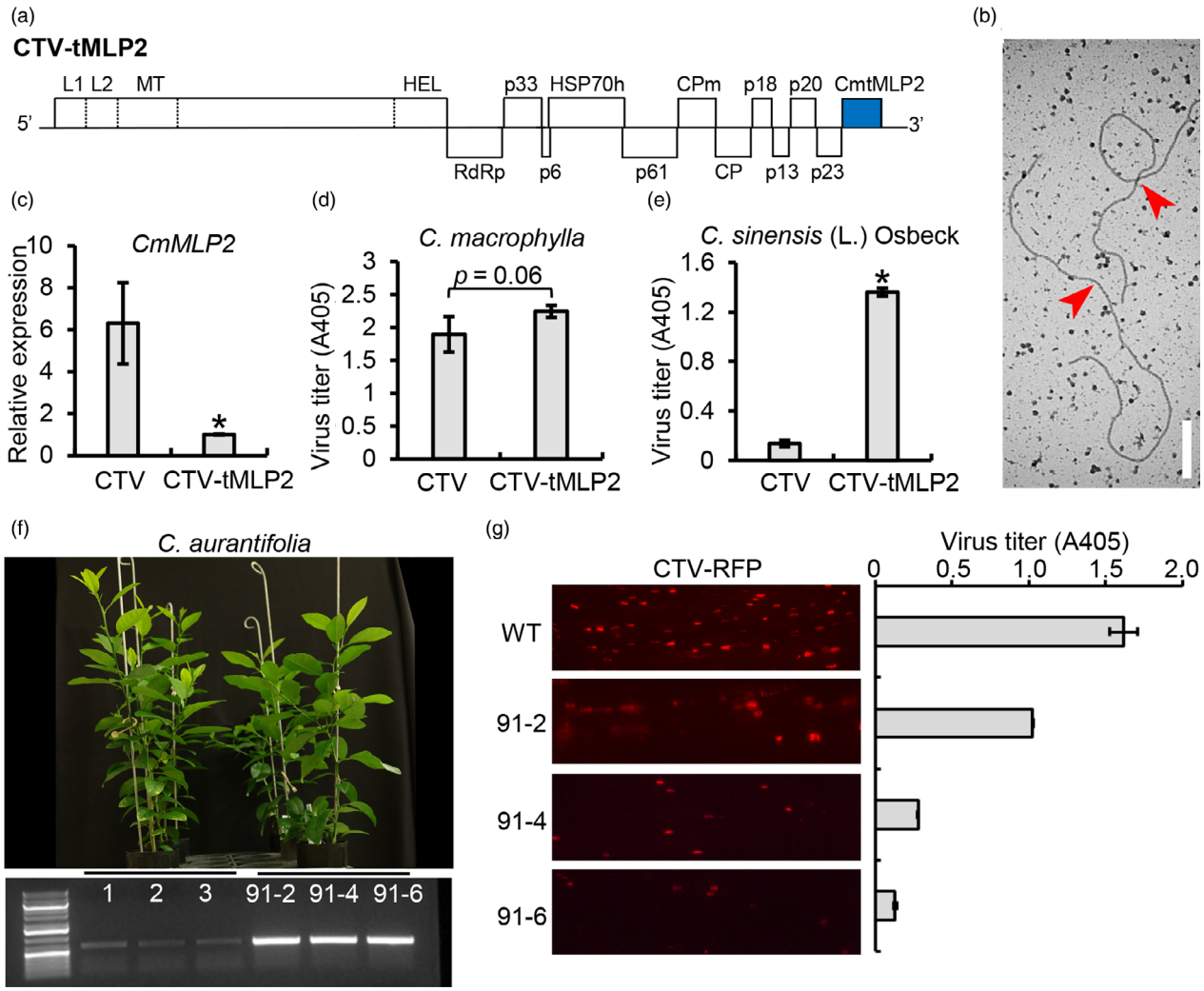

Figure 2 CmMLP2 is involved in defence against CTV infection. (a), The schematic representation of the CTV-tMLP2 construct. (b), Transmission electron microscopy observation of CTV-tMLP2 virions. Red arrows point to the positions of CTV virions. Bar = 200 nm. (c), The efficiency of citrus *MLP2* silencing via a CTV-based virus-induced gene silencing approach in *C. macrophylla* plants. Values represent the mean ± SD (n = 3). The asterisk indicates statistically significant differences as determined by Student's t-test (*, $P < 0.05$). (d), Virus titres of wild-type CTV and CTV-tMLP2 in the *C. macrophylla* plants assessed via enzyme-linked immunosorbent assay (ELISA). (e), Virus titres of wild-type CTV and CTV-tMLP2 in the *C. sinensis* (L.) Osbeck plants assessed via ELISA. (f), Generation of CmMLP2 overexpression transgenic *C. aurantifolia* lines (OEMLP2). The transcript levels of CmMLP2 in these plants were verified by semi-quantitative RT-PCR. (g), OEMLP2 lines showed increased resistance to CTV infection. Left row: Fluorescence observation of the CTV-RFP distribution in the bark of OEMLP2 lines and the wild-type control plants. Right row: CTV-RFP titre in the OEMLP2 lines and control plants.

systemic invasion. At six mpi, more than 80% of citrus plants inoculated with CTV-GFP:Δp33 became infected.

Altogether, our data showed that the CTV p33 protein is a movement-associated protein that influences the efficiency of the CTV systemic spread in the plant hosts.

Deletion of the CmMLP2 domain responsible for the protein interaction with p33 alleviates the CmMLP2-mediated defence response against CTV infection

To assess whether hijacking of p33 by CmMLP2 plays a role in the host interference with CTV infection, we examined how elimination of the ability of CmMLP2 to bind p33 affects virus infectivity. At first, we determined which domain(s) of CmMLP2 is responsible for p33 binding. Three portions of CmMLP2, which include a signal peptide (SP), a Kunitz motif (Ktz) and a cysteine-rich domain (Cys) (Fig. S2), were co-expressed with p33ΔTMD in the yeast. Through pairwise Y2H screening, we found that the cysteine-rich domain of CmMLP2 interacts with p33 (Figure 5a). To confirm the Cys-p33 interaction *in planta*, Co-IP was applied. However, a recombinant mGFP-tagged Cys protein appeared highly aggregated in *N. benthamiana* and remained insoluble in the Co-IP buffer (its solubilization was achieved only by adding a high concentration of urea), preventing its use in the assay (Fig. S8A, B). Therefore, as an alternative, a CmMLP2-mGFP mutant lacking the Cys domain (CmMΔCys-mGFP) was tested. In contrast with CmMLP2-mGFP, CmMΔCys-mGFP could not co-immunoprecipitate with RFP-p33 (Figure 5b). Furthermore, CmMΔCys-mGFP lost its ability to alter the subcellular distribution of RFP-p33 (Figure 5c). These observations confirmed that the Cys domain is required for the CmMLP2-p33 binding *in planta* as well as for the ability of CmMLP2 to alter the intracellular localization of p33.

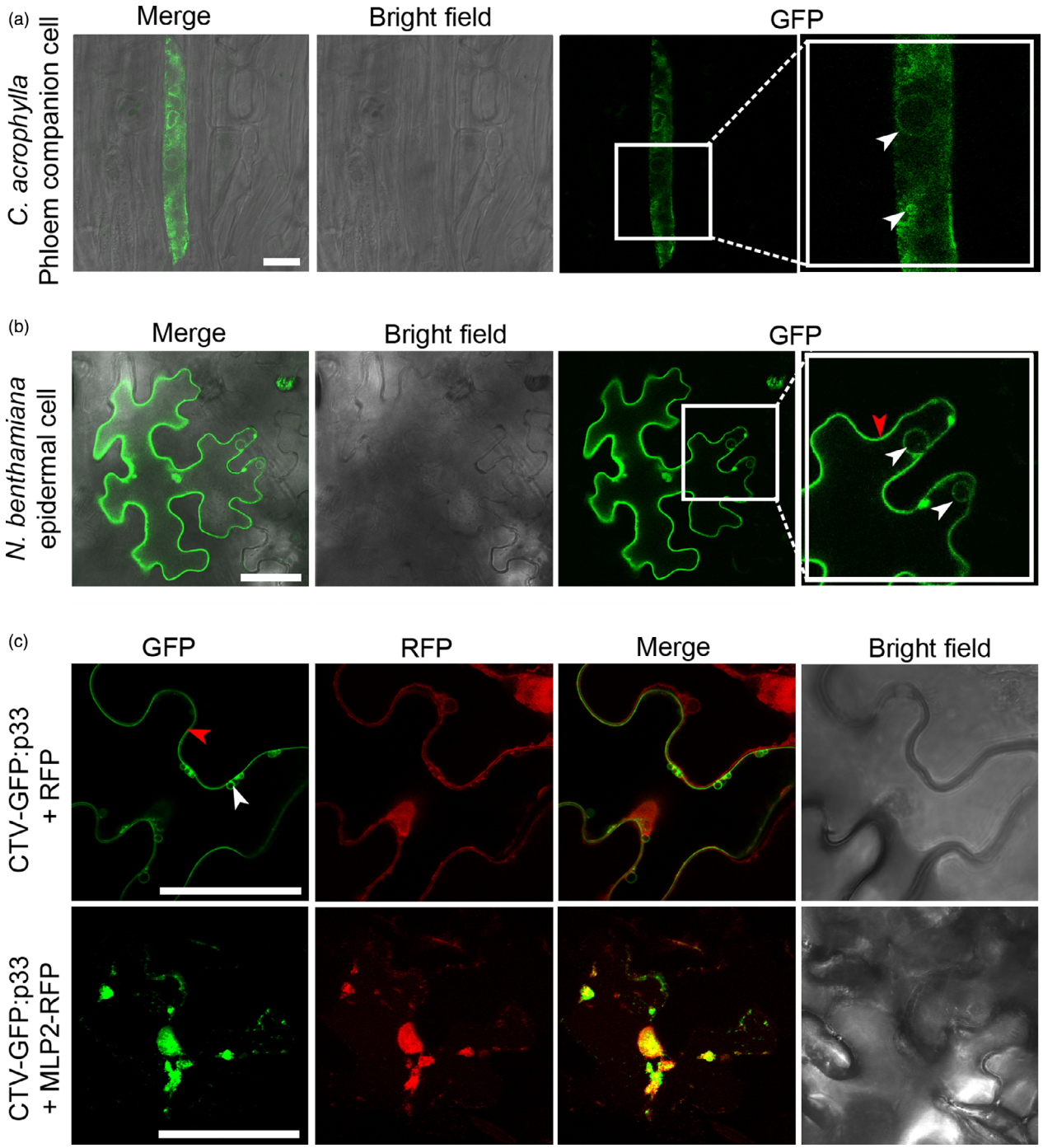

Figure 3 CmMLP2 alters the subcellular distribution of the p33 protein. (a), (b), Examination of the subcellular localization of GFP-p33 in the *C. macrophylla* phloem companion cells and *N. benthamiana* epidermal cells. Expression of GFP-p33 was driven by a CTV variant expressing GFP-p33 (CTV:GFP-p33) under the native p33 sgRNA promoter. White arrows point the vesicular structures formed by GFP-p33. Red arrows indicate the membrane localization of p33. Bar = 50 μm. (c), Observation of the effect of RFP and CmMLP2-RFP on the subcellular distribution of GFP-p33. The epidermal cells of *N. benthamiana* leaves were infiltrated with *Agrobacterium* cells harbouring the respective constructs. The images were captured by confocal microscopy. Bar = 50 μm.

Next, the free mGFP, CmMLP2-mGFP, and CmMΔCys-mGFP were co-expressed with CTV-GFP in *N. benthamiana*. As expected, at four wpi, CTV-GFP established a systemic infection and invaded the vascular tissue in the upper leaves of the plants in the free mGFP control set. Statistical analysis of 30 plants per treatment showed that over 90% of the control plants became successfully infected by CTV. However, the transient overexpression of CmMLP2 in the infiltrated leaves prevented the spread of CTV-GFP to the upper leaves in the plants. In comparison, CmMΔCys exhibited a decreased capability to hamper the CTV-GFP systemic infection: approximately 30% of plants became systemically infected by the virus, compared to none that got

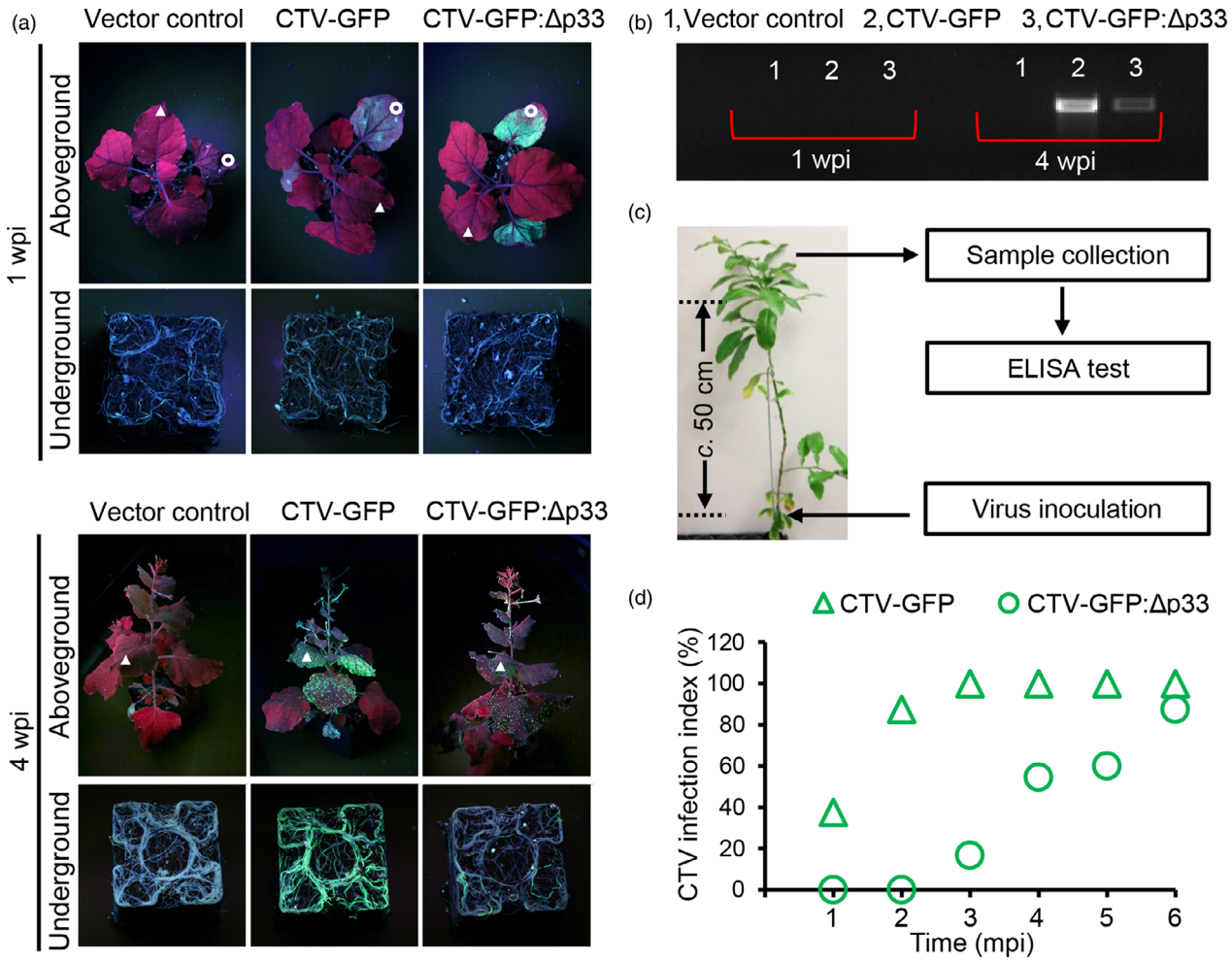

Figure 4 Observation of the systemic spread of CTV and CTV:Δp33 in virus-inoculated hosts. (a), Examination of the GFP fluorescence in *N. benthamiana* plants that were infiltrated with *Agrobacterium* expressing CTV-GFP and CTV-GFP:Δp33 at 1-week and 4-week post-infiltration. The images were taken by Canon T6 digital camera under the UV light. The white circles highlight the infiltrated leaves; the white triangles indicate the upper non-infiltrated leaves. (b), Assessment of the virus titre in the systemic upper leaves of *N. benthamiana* plants shown in (a) through semi-quantitative RT-PCR. A total of 10 ng total RNA was used as a template, and 25 cycles were run. (c), Schematic representation of a method used to conduct the 'virus-racing' assay in *C. macrophylla*. (d), Virus infection index of CTV and CTV:Δp33 during 6-month post-inoculation in *C. macrophylla*. Green triangles stand for the portion of plants infected by CTV-GFP; green circles stand for the percentage of plants infected by CTV-GFP:Δp33.

infected upon co-expressing the full-length CmMLP2 (Figure 5d, e, f), which correlated with inability of this CmMLP2 mutant to hijack p33.

Deletion of the Cys domain responsible for p33 binding only partially alleviated the function of CmMLP2 in defence against CTV, suggesting that the other two domains of CmMLP2 could also play important roles. Further observation of *N. benthamiana* plants that were inoculated with *Agrobacterium* expressing CTV-GFP along with the cultures expressing the mGFP-tagged SP or Ktz of CmMLP2 (SP-mGFP or Ktz-mGFP) showed that overexpression of Ktz had minimal effect on the systemic spread of CTV-GFP. Yet, the overexpressed SP could partially prevent virus systemic infection, as approximately 30% of plants were infected in the corresponding treatment (Figure 5d, e, f). Our observations suggest that the Kunitz motif of CmMLP2 may not be critical for the CmMLP2-mediated defence against CTV, while both the cysteine-rich domain and the signal peptide contribute to interference with CTV infection.

Ectopic expression of CmMLP2 triggers cellular stress by amalgamating the endoplasmic reticulum and the Golgi apparatus in *N. benthamiana*

The involvement of the short SP domain of CmMLP2 in defence against CTV suggested that, in addition to hijacking p33 and interfering with its function in virus movement, CmMLP2 could trigger other host immunity pathways to impede CTV systemic infection. The SP contains 25 amino acids and is highly conserved in the citrus MLPs (Fig. S2). To dissect the underlying mechanism, we next observed the subcellular localization of SP and the full-length CmMLP2. By co-expressing the mGFP-tagged SP or CmMLP2 along with several organelle markers in *N. benthamiana* by agroinfiltration, we found that SP and CmMLP2 were both localized at the ER and the Golgi apparatus. At three dpi, SP-mGFP and CmMLP2-mGFP exhibited a pattern that matched the distribution of the red fluorescence of a Golgi apparatus-specific marker, RFP-tagged α-1,2 mannosidase I, and an ER-specific

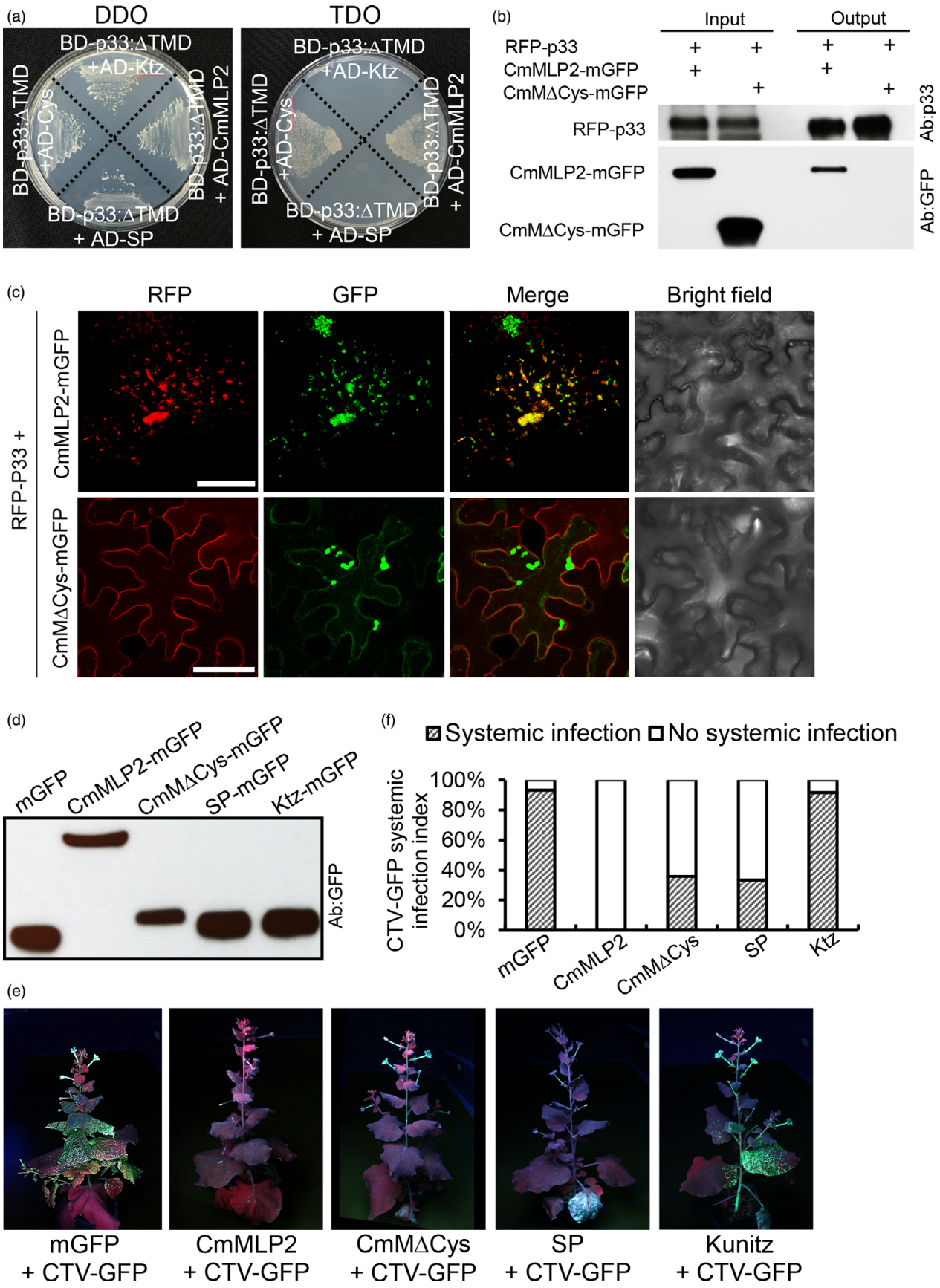

Figure 5 Functional examination of the involvement of the CmMLP2 domains in defence against CTV. (a), Pairwise yeast two-hybrid screening assay. The p33 protein without its transmembrane domain (p33ΔTMD), as bait, was co-expressed with full-length CmMLP2 and its three domains individually, as preys, in the golden yeast cells. The transformant yeast cells were screened in on SD/-Leu/-Trp DO (DDO) medium and SD/–Leu/–Trp/–His DO (TDO) medium for 72 h. SP: signal peptide; Ktz: Kunitz motif; Cys: domain containing conserved cysteines. (b), Co-immunoprecipitation assay. RFP-p33 was used as a bait, CmMLP2-mGFP and an mGFP-tagged CmMLP2 mutant lacking the Cys domain (CmMΔCys-mGFP) was used as prey. A p33-specific antibody was used to detect RFP-p33. The GFP-specific antibody was applied to detect CmMLP2-mGFP and CmMΔCys-mGFP. (c), Subcellular distribution of RFP-p33 co-expressed with CmMLP2-mGFP or CmMΔCys-mGFP. Yellow fluorescence indicates the colocalization of the two fluorescent protein-tagged partners. Bar = 50 μm. (d), Immunoblotting analyses using the GFP antibody to confirm the expression of CmMLP2-mGFP mutants. (e), Examination of the function of various CmMLP2 truncations in defence against CTV systemic infection in *N. benthamiana*. The six-week-old *N. benthamiana* plants were infiltrated with *Agrobacterium GV3101* harbouring the CTV-GFP construct (OD600 = 0.1) along with various CmMLP2 truncations in (c) (OD600 = 1.0). The distribution of CTV-GFP in the veins of upper leaves of *N. benthamiana* was observed under UV light in the darkroom. (f), The systemic infection index of CTV-GFP in *N. benthamiana* plants shown in (e). At least 30 plants were used in each treatment for calculation.

marker, RFP-tagged ER luminal retention signal HDEL (Goodin *et al*., 2007) (Figure 6a, b, c). Remarkably, in the free mGFP control set, both the ER and the Golgi apparatus had a typical appearance: the ER was seen as a thin-filament network throughout the cell, while the Golgi apparatus appeared forming small vesicles in the cytoplasm. In contrast, upon the ectopic expression of SP and CmMLP2, the ER and Golgi apparatus were visualized as dense aggregations in the cell.

The amalgamation of the ER and the Golgi apparatus resulting in the formation of aggregations is a functional disruption of the endomembrane system in the cell. While the mechanism of Golgi stress remains unexplored, the signal transduction cascade activated during ER stress is well characterized. To alleviate ER stress, host cells rely on the unfolded protein response (UPR) (Howell, 2013; Ron and Walter, 2007; Zhang and Wang, 2012). Hence, the genes involved in UPR could be used as markers for the host ER stress. The RT-qPCR analysis demonstrated that the relative expression of three UPR-related genes (Ye *et al*., 2011), *ER luminal-binding protein 4* (*BLP4/Bip4*), *Calreticulin* (*CRT*) and *protein disulphide-isomerase precursor* (*PDI*) in *N. benthamiana* increased dramatically upon CmMLP2-mGFP expression, compared to that of the mGFP control (Figure 6d).

Collectively, these results indicated that ectopic expression of CmMLP2 triggers cellular stress by amalgamating the ER and the Golgi apparatus in *N. benthamiana*.

The cellular stress triggered by CmMLP2 leads to ROS accumulation, which inhibits CTV replication in the host

Observation of the *N. benthamiana* leaves expressing mGFP, SP-mGFP, and CmMLP2-mGFP through agroinfiltration at 14 dpi showed that CmMLP2-mGFP and SP-mGFP but not the free mGFP triggered a PCD-like phenotype in the inoculated leaf patches (Figure 7a). Yet, expression of a CmMLP2 mutant without its SP sequence (*pCmMΔSP-mGFP*) in *N. benthamiana* could not trigger necrosis (Figure 7a). Previous findings proposed a positive feedback loop between ER stress and ROS accumulation, which acts as a regulator of PCD in plants (Ozgur *et al*., 2018). As expected, DAB staining resulted in the development of a dark brown colour in the leaf patches expressing CmMLP2-mGFP or SP-mGFP, indicating a significantly higher production of ROS in the corresponding patches, compared to that in the areas expressing the mGFP control or CmMΔSP-mGFP (Figure 7a, b). The role of SP in the induction of ROS was further confirmed by the observation that other CmMLP2 mutants, which lacked the Ktz or Cys domain but retained SP, showed the ability to trigger necrosis and ROS accumulation in *N. benthamiana*, in contrast with CmMΔSP-mGFP (Fig. S9). Next, we tested if up-regulation of CmMLP2 could trigger a similar response in the citrus plants. The leaves of three CmMLP2-overexpressing *C. aurantifolia* lines (OEMLP2:91-2, OEMLP2:91-4, OEMLP2:91-6) were subjected to DAB staining. As shown in Fig. 7C, D, the leaves collected from the transgenic lines exhibited a darker brown colour, compared to that of the wild-type control, especially, in the vasculature of the leaves, though the difference between 91-2 and the control was not statistically significant ($P = 0.056$). Furthermore, DAB staining of the citrus tissue from trees infected by the wild-type CTV and CTV-tMLP2 demonstrated that CTV-tMLP2 infection triggered less accumulation of ROS, compared to the wild-type CTV infection (Figure 7e, f). These assays indicated that CmMLP2 is a regulator of ROS.

ROS accumulation is an effective plant basal defence strategy against CTV infection (Sun and Folimonova, 2019). Therefore, we tested if the CmMLP2-mGFP or SP-mGFP expression could restrict the replication of CTV by co-infiltrating *Agrobacterium* cultures harbouring the CTV construct ($OD_{600} = 0.1$) along with those harbouring *pmGFP*, *pCmMLP2-mGFP*, *pCmMΔSP-mGFP*, or *pSP-mGFP* ($OD_{600} = 1.0$) in *N. benthamiana*. The virus titre in the inoculated leaves was quantified by RT-qPCR at 7 dpi. CTV generated less viral RNA copy numbers when it was co-expressed with CmMLP2-mGFP or SP-mGFP, compared to that in the leaves expressing mGFP or CmMΔSP-mGFP (Figure 7g).

Altogether, our observations suggested that SP is the key domain that endows the CmMLP2 ability to trigger ROS accumulation, which further hampers the CTV replication.

Discussion

MLPs belong to the soybean KTI super-family and have been isolated from different plants such as tomato, coffee, tobacco and citrus. In the past decade, several of them were implicated in plant defence against pathogens, yet the detailed mechanisms of their action remain elusive. It has been reported that *NbMLP1*, *NbMLP2* and *NbMLP3* could be induced following bacterial and fungal infections (*Pseudomonas syringae* and *Colletotrichum destructivum/C. orbiculare*) in *N. benthamiana* (Goodwin *et al*., 2012). LeMLP was required for Cf-4/Avr4- and Cf-9/Avr9-dependent hypersensitive cell death in the tomato (*Lycopersicon esculentum*)-*Cladosporium fulvum* pathosystem (Xu *et al*., 2012). The expression profiles of MLP1 and MLP3 change upon mite (*Tetranychus urticae*) infection in citrus (Podda *et al*., 2014). Furthermore, earlier transcriptomic and proteomic analyses reported that expression of citrus MLP2 could be induced upon CTV infection; however, the role of MLP2 in the citrus-CTV interactions remained unexplained (Dória *et al*., 2015; Gandía

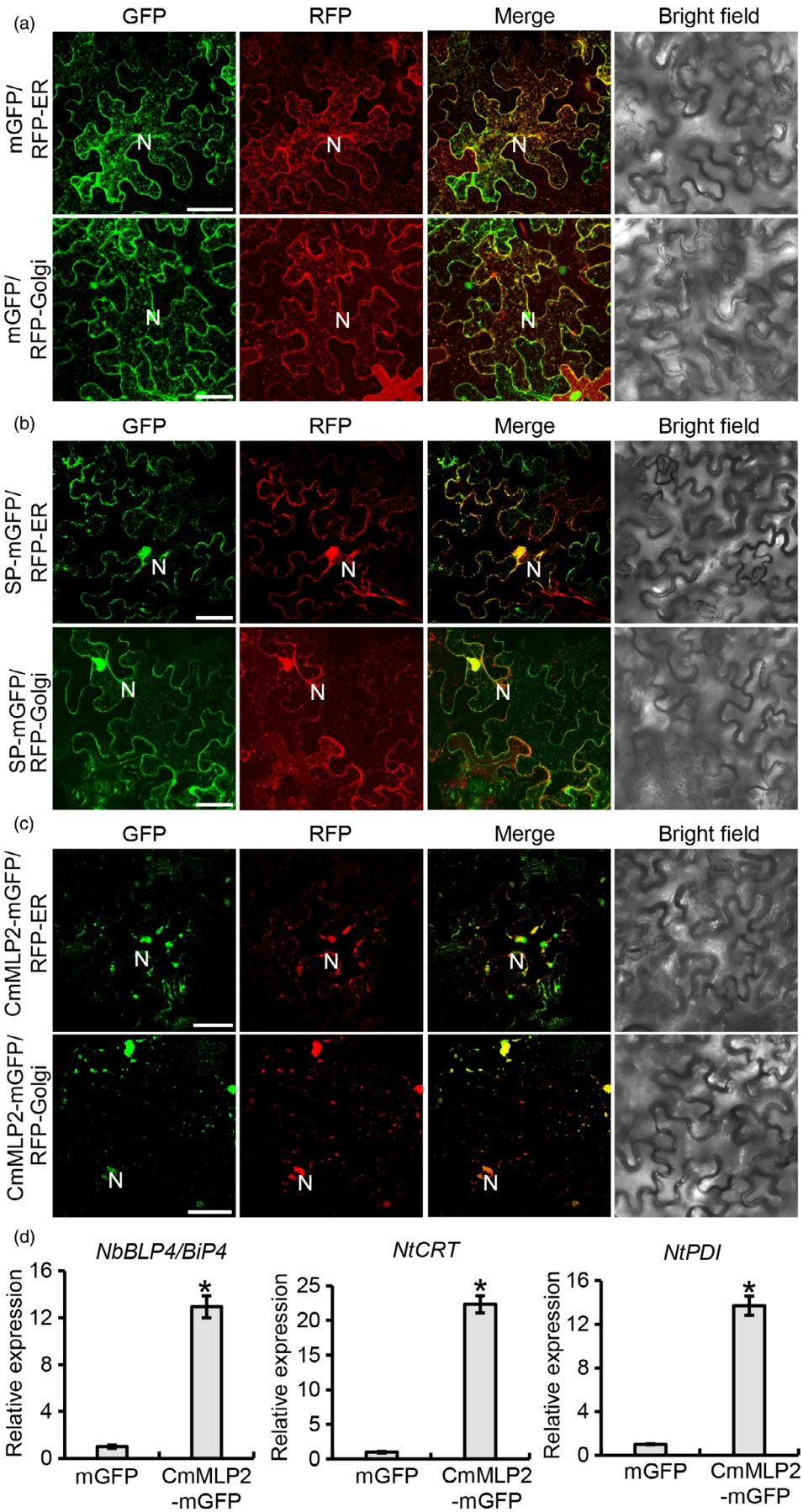
(a)
GFP
RFP
Merge
Bright field
mGFP/ RFP-ER
mGFP/ RFP-Golgi
N
(b)
SP-mGFP/ RFP-ER
SP-mGFP/ RFP-Golgi
(c)
CmMLP2-mGFP/ RFP-ER
CmMLP2-mGFP/ RFP-Golgi
(d)
NbBLP4/BiP4
NtCRT
NtPDI
Relative expression
mGFP
CmMLP2 -mGFP
*

Figure 6 Overexpression of CmMLP2 amalgamates the endoplasmic reticulum (ER) and the Golgi apparatus in the *N. benthamiana* plants. (a), (b) and (c), Observation of the subcellular localization of CmMLP2 in the epidermal cells of *N. benthamiana* leaves. Plants were infiltrated with *Agrobacterium* harbouring free mGFP, as control, SP-mGFP, or CmMLP2-mGFP along with the RFP-tagged ER luminal retention signal HDEL (RFP-ER) or RFP-tagged α-1,2 mannosidase (RFP-Golgi) as markers. Images were captured using confocal microscopy. N, nucleus. Bar = 50 μm. (d), Expression profiles of the ER stress-related genes assessed by RT-qPCR in the mGFP control and CmMLP2-mGFP overexpression leaves. *NbBip*: *ER luminal-binding protein 4*; *NtCRT*: *Calreticulin*; *NtPDI*: *Protein disulphide-isomerase precursor*. Values represent means ± SD (n = 3) (*, $P < 0.05$, Student's *t*-test). A similar tendency was obtained from at least three biological repeats.

et al., 2007). In this study, we demonstrated that citrus MLP2 functions in defence against CTV invasion and dissected the potential underlying mechanism. Although this mechanism appears not to be robust enough to provide complete host resistance against CTV, it negatively affects the efficiency of virus systemic spread and the virus titre. These data expand the role of MLPs as broad-spectrum antimicrobial peptides mediating plant defence against viruses.

As an elicitor of the up-regulation of the host MLP2, a non-conserved p33 protein of CTV has been shown to be a multifunctional protein (Folimonova, 2020). In particular, it was demonstrated that p33 possesses certain characteristics of the viral movement proteins and is required for infection of selective citrus hosts (Bak and Folimonova, 2015; Tatineni *et al*., 2011). However, how p33 is involved in the CTV movement remained elusive. In this study, we showed that deletion of the p33 ORF in the CTV genome interfered with the speed of the virus translocation to the un-inoculated distal plant tissue, which suggested that p33 influences the efficiency of the systemic spread of CTV. Thus, p33, an effector of CTV, is a movement-associated protein. In a number of plant host–virus systems, it has been shown that virus movement-associated proteins could act as viral effectors and be targeted by the host immunity. For instance, the tobamovirus *Tomato mosaic virus* movement protein is recognized by the R gene products Tm-2 and Tm-2^2, which result in the induction of the plant defence reaction (Meshi *et al*., 1989; Weber *et al*., 2004). The *Tobacco mosaic virus* movement protein was reported to modulate plant biotic stress responses in *N. tabacum* (Conti *et al*., 2012). In the citrus-CTV pathosystem, the movement-associated p33 protein was targeted by the host CmMLP2 whose accumulation markedly altered the cellular distribution of p33. The hijacked p33 was no longer observed forming cytoplasmic vesicles known to be one of the characteristics of viral movement proteins and, instead, appeared in large aggregations. Deletion of the p33-binding domain in CmMLP2 alleviated its function in defence against CTV. The evidence suggests that interruption of the p33 function(s) by CmMLP2 contributes to limiting the systemic spread of the virus in its hosts.

The ability of CmMLP2 to hijack p33 relies on its ability to amalgamate the ER and the Golgi apparatus. It is known that the interference with the endomembrane trafficking system triggers cellular stress, which is closely related to ROS signalling in the plant cells (Ozgur *et al*., 2018). In this study, we showed that while overexpression of CmMLP2 stimulated ROS accumulation, which provokes PCD in the hosts, a knock-down of the CmMLP2 expression reduced the ROS burst triggered by CTV. As broad-spectrum antimicrobial compounds, ROS function in defeating invasion of pathogens, including fungi, bacteria, nematodes and viruses (Torres *et al*., 2006). As a regulator of ROS, it seems plausible that citrus MLP2 also appears to be involved in defence against other phloem-limited citrus pathogens such as *Candidatus* Liberibacter asiaticus (Bowman and Albrecht, 2013; Nwugo *et al*., 2016) and *Ca*. Phytoplasma aurantifolia (Taheri *et al*., 2011). Earlier, we have reported that a high concentration of ROS prevents CTV multiplication (Sun and Folimonova, 2019). In accordance with this observation, we found that ROS triggered by MLP2 suppressed the accumulation of CTV in the plants. Based on the evidence, we suggest that CmMLP2 mediates defence against CTV infection by modulating the host oxidative stress and, specifically, ROS accumulation, to suppress virus multiplication. Surprisingly, a predicted Kunitz motif of CmMLP2 was not involved in such host responses, but the short signal peptide was. The underlying signal cascade remains unknown and requires further investigation.

In summary, our study demonstrates a dual function of citrus MLP2 in defence against CTV (Figure 7h). The accumulation of MLP2 triggered by the p33 protein upon citrus infection by CTV amalgamates the ER and Golgi apparatus and leads to the formation of condensed aggregations, resulting in cellular stress and ROS production. The elevated cellular stress and ROS suppress the multiplication of CTV in the virus-infected cells and reduce the virus titre. Additionally, binding of MLP2 to the p33 protein alters the endomembrane distribution of p33, which is crucial for the proper function of this viral protein. As p33 facilitates virus movement in the phloem, its hijacking by citrus MLP2 impedes the efficiency of the establishment of virus systemic infection in the host. Given that the CmMΔCys mutant still reorganizes the cellular endomembrane system and induces aggregations, while it cannot alter the subcellular distribution of p33 (Figure 5c), the MLP2-mediated hijacking of p33 depends on the MLP2-p33 interaction and is independent of the CmMLP2-caused endomembrane stress and cell death. Therefore, a phloem-localized citrus MLP2 empowers a two-way defence to hamper CTV infection.

Experimental procedures

Plasmid constructs

The CTV strain T36 was used in this study. All the infectious cDNA clones of CTV variants were driven by the cauliflower mosaic virus (CaMV) 35S promoter in a binary vector pCAMBIA1380. To generate *pCTV-tMLP2*, a truncated *CmMLP2* gene (*tMLP2*) was used to replace the sequence of a truncated *PDS* gene in the backbone of *pCTV-tPDS* (Hajeri *et al*., 2014). To generate mGFP-tagged CmMLP2 truncations, DNA sequences encoding various CmMLP2 fragments were sub-cloned into the binary vector *pCAMBIA 1300s*, which was modified by adding a *mTagGFP* gene at the 3′ terminus of the multiple cloning site (Wang *et al*., 2017). To generate the constructs expressing free RFP or CmMLP2-RFP, the DNA sequences encoding RFP or CmMLP2-RFP were obtained and cloned under the control of the 35S promoter into the plant expression vector *pCASS-4N*. All primers used for engineering constructs are listed in Table S1.

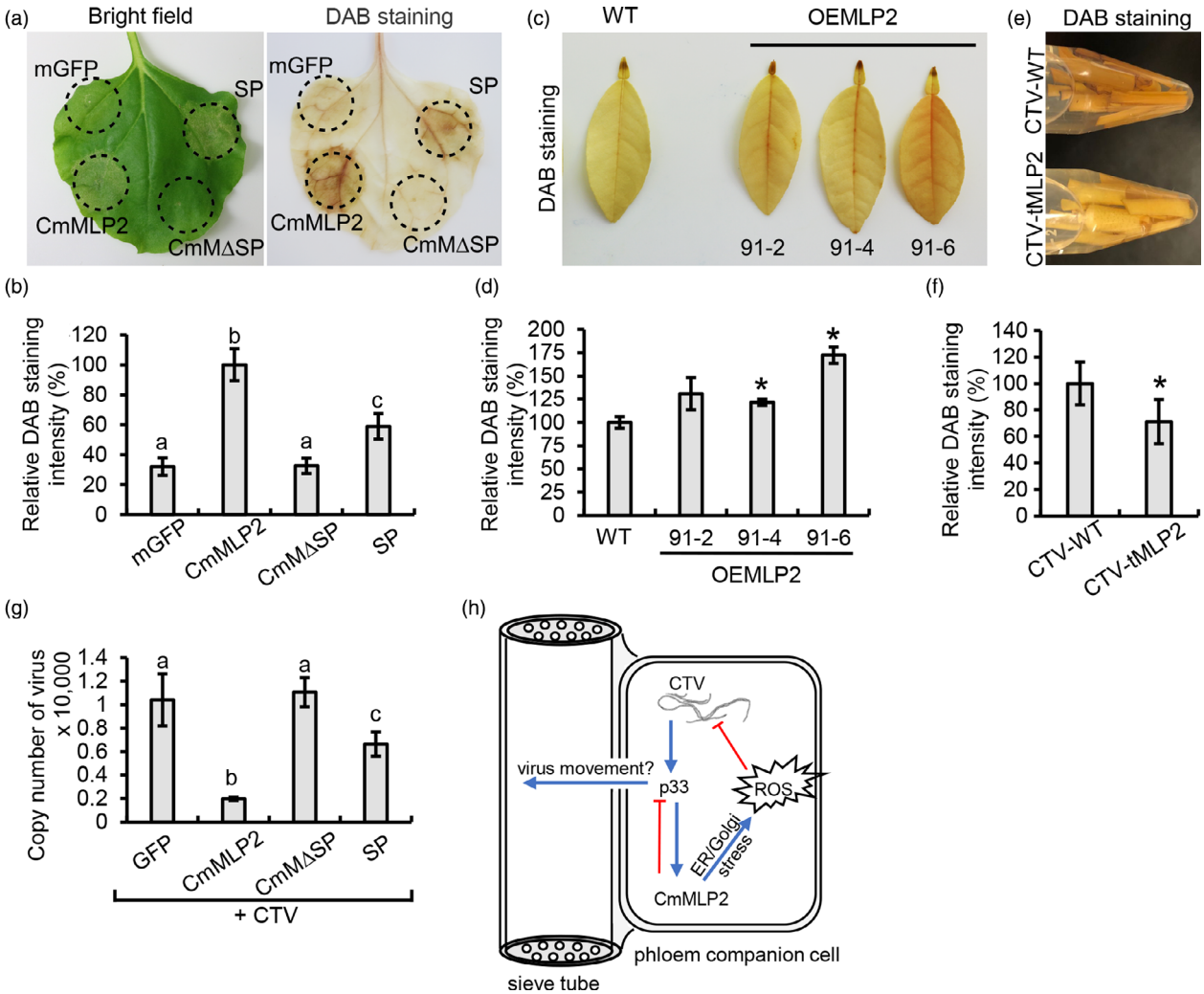

Figure 7 ROS accumulation triggered by the up-regulation of CmMLP2 inhibits CTV multiplication. (a), Observation of the production of the most abundant ROS, hydrogen peroxide, in *N. benthamiana* leaves infiltrated with *Agrobacterium* harbouring *pmGFP*, *pCmMLP2-mGFP* (CmMLP2), *pCmMΔSP-mGFP* (CmMΔSP), or *pSP-mGFP* (SP) binary constructs using DAB staining. (b), The relative colour intensity of the DAB staining in (A). At least three representative images were chosen for the measurement. The different letters indicate statistically significant differences ($P < 0.01$, Student's *t*-test). (c), CmMLP2 overexpression transgenic *C. aurantifolia* lines (OEMLP2) show higher ROS accumulation, compared to that of the wild-type control. (d), The relative colour intensity of the DAB staining in (C). The asterisk indicates statistically significant differences as determined by Student's *t*-test (*, $P < 0.05$). (e), CTV-tMLP2 triggers less ROS accumulation in the *C. macrophylla* plants, compared to that induced by the wild-type CTV. Young stems were subjected to DAB staining. (f), The relative colour intensity of the DAB staining in (e). (*, $P < 0.05$, Student's *t*-test). (g), Quantification of the CTV genomic RNA in the leaf patches shown in (a). Different letters stand for statistically significant differences. ($P < 0.05$, Student's *t*-test). (h), Schematic model of the dual function of CmMLP2 in defence against CTV in the citrus phloem-associated cells.

Plant material and virus inoculation

The citrus varieties, *C. macrophylla*, *C. aurantifolia* and *C. sinensis* (L.) Osbeck, were grown in the greenhouse conditions in Gainesville, FL, USA. To generate the overexpression transgenic citrus lines, the ORFs of *p33* and *CmMLP2* were inserted into the binary expression vector *pCAMBIA-2301*. An ORF of *GFP* under the CaMV 35S promoter was added in the construct to facilitate initial screening of the citrus transformants due to the low transformation efficiency. The overexpression constructs were then transformed into *A. tumefaciens* strain *EHA105*, and the *A. tumefaciens*-mediated transformation was conducted to generate *C. macrophylla* or *C. aurantifolia* transgenic lines as described in Orbović and Grosser (2015).

The 'bark-flap' inoculation method was applied to inoculate citrus plants. Briefly, the six-week-old *N. benthamiana* plants were infiltrated with *A. tumefaciens* strain *GV3101* (OD_{600} = 0.1) harbouring the recombinant *pCAMBIA-1380-CTV* plasmid vectors. The intact virions were purified by ultracentrifugation using sucrose cushion (Robertson *et al.*, 2005) and then were inoculated into citrus trees by putting the suspension under the bark. As for the 'graft' inoculation, a budwood collected from a citrus source plant bearing a CTV variant was used to graft into the receptor trees.

TEM imaging

The images of CTV virions were taken using Hitachi H-7000 TEM (Hitachi High-Technologies, Japan) equipped with Veleta

(2 k × 2 k) CCD side mount camera (EMSIS, Germany) at 100 kV. Briefly, drops of virions-containing suspension mentioned above were applied onto 400-mesh copper grids (Formvar/Carbon Square Mesh, UB, Electron Microscopy Sciences, USA) to capture the virions. The grids were stained using 1% uranyl acetate for 30 s. The dried grids were subjected to TEM observations.

Plant photography and fluorescence stereomicroscopy imaging

The examination of a fluorescent protein-tagged CTV variants—CTV-GFP, or CTV-GFP:Δp33—in *N. benthamiana* plants (underground or aboveground) was conducted in the darkroom using a handheld UV lamp (365 nm, UVP, Upland, CA). Images were taken using a Canon T6 digital camera (Canon USA, Mason, VA) by a time-lapse exposure setting.

The distribution of CTV-RFP in the phloem-associated tissue of *C. aurantifolia* and that of CTV:GFP-p33 in the *C. macrophylla* stems was visualized using a fluorescence stereo microscope Leica M165 FC (Leica Microsystems) and hand-cut tissue samples. The built-in RFP channel was used to excite the RFP fluorescence, and the long-GFP wavelength was used to excite the GFP fluorescence. Images were taken by digital colour camera Leica DFC310 FX.

ELISA

Double antibody sandwich-indirect ELISA was used to test infection of CTV in citrus trees. A total of 0.25 g of virus-infected citrus stem tissue was ground using 5 mL of the extraction buffer (3.2 mM Na_2HPO_4, 0.5 mM KH_2PO_4, 1.3 mM KCl, 135 mM NaCl, 0.05% Tween® 20, pH 7.4). Purified IgG from the rabbit polyclonal antibody CTV-908 (1 μg mL^{-1}) was used as a coating antibody, and the CTV monoclonal antibody ECTV172 was used as detecting antibody. The chromogenic reaction was developed in 45 mins in the dark, and the absorbance intensity was read at 405 nm (A405).

Protein expression and immunoblot analysis

Western blotting was used to confirm the expression of the CmMLP2-derived recombinant proteins in *N. benthamiana*. The recombinant proteins were transiently expressed in the plants through *Agrobacterium*-mediated transformation. At three dpi, the total protein was extracted from the infiltrated leaves by mixing 2M Urea solution (PH = 10) and an equal volume of 2x protein loading buffer (125 mM Tris pH 6.8, 4% w/v SDS, 40% v/v glycerol, 0.2% w/v bromophenol blue, 10 mM Dithiothreitol). The immunoblotting was performed using an anti-GFP antibody (Santa Cruz Biotechnology, TX) as a primary antibody (1 : 5000 dilution) and a horseradish peroxidase-conjugated anti-mouse IgG (Santa Cruz Biotechnology) as a secondary antibody (1 : 50 000 dilution). The signal was developed and visualized on a chemiluminescence film (X-OMAT LS; Carestream Kodak, Sigma-Aldric).

Similar methods were used to confirm expression of the p33 protein in the OEp33 transgenic *C. macrophylla* lines. A total of 150 mg of plant tissue was collected to extract the total protein. Western blotting was performed using a rabbit anti-p33 serum as a primary antibody (Kang *et al*., 2015) and a horseradish peroxidase-conjugated goat anti-rabbit IgG (Santa Cruz Biotechnology) as a secondary antibody.

RNA extraction, RT-PCR, and RT-qPCR

Total RNA from citrus and *N. benthamiana* plants was extracted using the Direct-zol™ RNA Kit (ZYMO RESEARCH). To evaluate the p33 transcripts in the OEp33 transgenic citrus lines, semi-quantitative RT-PCR was conducted following the instructions of SuperScript™ III One-Step RT-PCR System with Platinum™ Taq DNA Polymerase (Invitrogen). A total of 10 ng of total RNA was used as a template. The p33 specific primers were used to amplify the p33 transcript for 25 PCR cycles. Similarly, to quantify the CTV-GFP and CTV-GFP: Δp33 accumulation in the *N. benthamiana* upper leaves, CTV-specific primers (HEL-F and HEL-R) were used to amplify the respective fragment of the CTV genome.

The CTV genomic copy number was calculated using one-step quantitative RT-PCR method, as described previously (Bergua *et al*., 2016). A total of 1 ng of total RNA was used as a template. Two CTV-specific primers and 6-FAM/BHQ-1 labelled TaqMan® probe were used to amplify the specific region between the RNA-dependent RNA polymerase and p33 ORFs. The relative expression of the citrus *MLP2* gene in citrus plants was tested by a two-step RT-qPCR method. Briefly, 2 μg of total RNA was used to synthesize cDNA according to the protocol of the GoScript™ Reverse Transcription System (Promega). SsoAdvanced™ Universal SYBR® Green Supermix (BIO-RAD) and a real-time PCR detection system (CFX96 Touch) were used to run the PCR. *Citrus ubiquitin 10* (*UBQ 10*) was set as an internal control. Similarly, the relative expression of genes involved in ER stress or UPR was also tested by the two-step RT-qPCR method. The *N. benthamiana* samples were taken at seven days post-*Agrobacterium* infiltration. The *UBQ* gene in *N. benthamiana* was used as an internal control. Primers and probe listed above are listed in Table S1. Similar results were obtained from three independent assays.

Y2H assays

The Y2H assay was performed according to the Matchmaker® Gold Yeast Two-Hybrid System User Manual (Clontech, Takara Bio). Briefly, total RNA from CTV-infected *C. macrophylla* stems was extracted to produce a cDNA library, which was further cloned into the yeast expression vector *pAD* (*pGADT7*) for screening prey proteins. The coding sequence of p33ΔTMD was constructed in the *pBD* vector (*pGBKT7*) as a bait (Kang *et al*., 2017).

The pairwise Y2H was applied to validate the interaction between p33ΔTMD and CmMLP2 as well as its truncations. The cDNAs encoding two polypeptides were cloned into *pAD* and *pBD* vectors, respectively. The vector construct *pGBKT7-53* was set as a positive control bait plasmid; *pGBKT7-Lam* was used as a negative control bait plasmid; and *pGADT7-T* was set as a positive control prey plasmid. Next, the respective combinations of plasmids were co-transformed into the yeast cells and cultured on SD/-Leu/-Trp DO (DDO) medium. Upon cultivating the transformants at 30°C for 72 h, the independent colonies were further selected on SD/–Leu/–Trp/–His DO (TDO) medium, or SD/–Leu/–Trp/–Ade/–His DO (QDO) medium, or SD/-Leu/-Trp DO (DDO) medium plus 200 ng/mL Aureobasidin A and 40 μg/mL X-a-Gal (DDO/X/A).

Co-IP assays

Co-IP assays were performed as described in the protocol for RFP-Trap® Agarose (Chromotek, Martinsried, Germany). Briefly, RFP-p33, which acts as a bait, was co-expressed with free mGFP, CmMLP2-mGFP, or CmMΔCys-mGFP by agroinfiltration, respectively, in *N. benthamiana*. *Agrobacterium* culture harbouring wild-type CTV (OD_{600} = 0.1) construct was introduced simultaneously to create a similar cellular environment with the physiological viral infection. At three dpi, the total protein was

extracted from *N. benthamiana* leaves and used to confirm the expression of the respective proteins as the input control. The RFP-Trap® Agarose beads were applied to capture the RFP-p33 protein. The eluted protein complexes were collected as output. The extracted proteins (input and output) were further separated on a 10% SDS-polyacrylamide gel and detected by immunoblot using anti-p33 (Ab:p33) or anti-GFP antibodies (Ab:GFP, Abcam, Cambridge, UK).

Laser scanning confocal microscopy imaging

The intracellular distribution of the mGFP- or RFP-tagged proteins in the epidermal cells of *N. benthamiana* leaves or citrus phloem companion cells was visualized using Leica TCS SP5 confocal laser scanning microscope system (Leica Microsystems). The GFP signal (excited at 488 nm) was collected at 550–600 nm. The RFP signal (excited at 555 nm) was collected at 600–630 nm. Images were captured using a 63X oil objective and processed using LAS-X (Leica Microsystems) software.

In situ hybridization

A full length of the *CmMLP2* sequence was subcloned into the *pSPT18* vector. The preparation of the *CmMLP2*-specific antisense probe labelled with digoxigenin-UTP was generated according to DIG RNA Labeling Kit (SP6/T7; Roche). Mature citrus stems infected with CTV were collected, fixed and embedded in paraffin. The *in situ* hybridization assay was conducted as described previously (Wang *et al*., 2013). Briefly, the hybridized probes anchored with digoxigenin were detected using the Anti-Digoxigenin-AP, Fab fragments (Sigma-Aldrich, St. Louis, MO) and 1-Step™ Nitro blue tetrazolium/5-Bromo-4-chloro-3-indolyl phosphate (Thermo Fisher Scientific, Waltham, MA) as substrates. Sections were imaged using Leica MZ10F fluorescence dissecting stereomicroscope.

Histochemical assays

DAB staining was conducted as described previously (Li *et al*., 2016). Briefly, *N. benthamiana* leaves and hand-cut citrus stem were directly stained with 1 mg/mL DAB-HCl solution (Sigma-Aldrich, St. Louis, MO) overnight. The samples were de-stained with ethanol. The relative DAB staining intensity was measured by ImageJ software (http://rsbweb.nih.gov/ij).

Acknowledgements

We thank Dr. Siddarame Gowda (Department of Plant Pathology, University of Florida) for technical assistance with a construct for the p33 overexpression lines and Dr. Subhas Hajeri (Central California Tristeza Eradication Agency, CA, USA) for providing us with the pCTV-tPDS vector. We are grateful to Dr. Vladimir Orbović (Core Citrus Transformation Facility, Citrus Research and Education Center, University of Florida) for technical assistance on generation the p33 and CmMLP2 overexpression transgenic citrus lines. This research was supported by the National Science Foundation under Grant no. 1615723 (to Svetlana Y. Folimonova). Any opinions, findings, and conclusions or recommendations expressed in this material are those of the author(s) and do not necessarily reflect the views of the National Science Foundation.

Conflict of interest

The authors declare no conflict of interest.

Author contributions

S. Y. F. and Y.-D. S. conceived and designed the study, participated in data analysis and interpretation, and drafted the manuscript. Y.-D. S., Z. L. and S. Y. F. performed the experiments. All authors read and approved the manuscript.

References

Atallah, O.O., Kang, S.H., El-Mohtar, C.A., Shilts, T., Bergua, M. and Folimonova, S.Y. (2016) A 5′-proximal region of the *Citrus tristeza virus* genome encoding two leader proteases is involved in virus superinfection exclusion. *Virology,* **489**, 108–115.

Bak, A. and Folimonova, S.Y. (2015) The conundrum of a unique protein encoded by *citrus tristeza virus* that is dispensable for infection of most hosts yet shows characteristics of a viral movement protein. *Virology,* **485**, 86–95.

Bergua, M., Kang, S.H. and Folimonova, S.Y. (2016) Understanding superinfection exclusion by complex populations of *Citrus tristeza virus*. *Virology,* **499**, 331–339.

Bowman, K.D. and Albrecht, U. (2013) Comparison of gene expression changes in susceptible, tolerant and resistant hosts in response to infection with *Citrus tristeza virus* and huanglongbing. *J. Citrus Pathol.* **2**, 30450.

Brouwer, J.N., Van Der Wel, H., Francke, A. and Henning, G.J. (1968) Miraculin, the sweetness-inducing protein from miracle fruit. *Nature,* **220**, 373–374.

Conti, G., Rodriguez, M.C., Manacorda, C.A. and Asurmendi, S. (2012) Transgenic expression of *Tobacco mosaic virus* capsid and movement proteins modulate plant basal defense and biotic stress responses in *Nicotiana tabacum*. *Mol. Plant Microbe Interact.* **25**, 1370–1384.

Dawson, W.O., Bar-Joseph, M., Garnsey, S.M. and Moreno, P. (2015) *Citrus tristeza virus*: making an ally from an enemy. *Annu. Rev. Phytopathol.* **53**, 137–155.

Dawson, W.O., Garnsey, S.M., Tatineni, S., Folimonova, S.Y., Harper, S.J. and Gowda, S. (2013) *Citrus tristeza virus*-host interactions. *Front. Microbiol.* **4** (88), 1–10.

Dolja, V.V., Kreuze, J.F. and Valkonen, J.P. (2006) Comparative and functional genomics of closteroviruses. *Virus Res.* **117**, 38–51.

Dória, M.S., Sousa, A.O., Barbosa Cde, J., Costa, M.G., Gesteira Ada, S., Souza, R.M., Freitas, A.C. *et al*. (2015) *Citrus tristeza virus* (CTV) causing proteomic and enzymatic changes in sweet orange variety "Westin". *PLoS One,* **10**, e0130950.

Folimonova, S.Y. (2012) Superinfection exclusion is an active virus-controlled function that requires a specific viral protein. *J. Virol.* **86**, 5554–5561.

Folimonova, S.Y. (2020) *Citrus tristeza virus*: A large RNA virus with complex biology turned into a valuable tool for crop protection. *PLoS Pathogen.* **16**(4), e1008416.

Gandía, M., Conesa, A., Ancillo, G., Gadea, J., Forment, J., Pallás, V., Flores, R. *et al*. (2007) Transcriptional response of *Citrus aurantifolia* to infection by *Citrus tristeza virus*. *Virology,* **367**, 298–306.

Goodin, M.M., Chakrabarty, R., Banerjee, R., Yelton, S. and Debolt, S. (2007) New gateways to discovery. *Plant Physiol.* **145**, 1100–1109.

Goodwin, P.H., Xie, W. and Valliani, M. (2012) Three genes of miraculin-like proteins from *Nicotiana benthamiana* with dissimilar putative structures show highly similar patterns of induction following bacterial and fungal infections. *Eur. J. Plant Pathol.* **134**, 795–810.

Hajeri, S., Killiny, N., El-Mohtar, C., Dawson, W.O. and Gowda, S. (2014) *Citrus tristeza virus*-based RNAi in citrus plants induces gene silencing in *Diaphorina citri*, a phloem-sap sucking insect vector of citrus greening disease (Huanglongbing). *J. Biotechnol.* **176**, 42–49.

Howell, S.H. (2013) Endoplasmic reticulum stress responses in plants. *Annu. Rev. Plant Biol.* **64**, 477–499.

Jones, J.D. and Dangl, J.L. (2006) The plant immune system. *Nature,* **444**, 323–329.

Kang, S.H., Bak, A., Kim, O.K. and Folimonova, S.Y. (2015) Membrane association of a nonconserved viral protein confers virus ability to extend its host range. *Virology,* **482**, 208–217.

Kang, S.H., Dao, T.N.M., Kim, O.K. and Folimonova, S.Y. (2017) Self-interaction of *Citrus tristeza virus* p33 protein via N-terminal helix. *Virus Res.* **233**, 29–34.

Karasev, A.V., Boyko, V.P., Gowda, S., Nikolaeva, O.V., Hilf, M.E., Koonin, E.V., Niblett, C.L. *et al*. (1995) Complete sequence of the *citrus tristeza virus* RNA genome. *Virology,* **208**, 511–520.

Li, Y.B., Han, L.B., Wang, H.Y., Zhang, J., Sun, S.T., Feng, D.Q., Yang, C.L. *et al*. (2016) The thioredoxin GbNRX1 plays a crucial role in homeostasis of apoplastic reactive oxygen species in response to *Verticillium dahliae* infection in cotton. *Plant Physiol.* **170**, 2392–2406.

Liu, Y., Li, F. and Liu, J.-Z. (eds). (2017) Plant immunity against viruses. *Front. Microbiol.* **8**, 520.

Lu, R., Folimonov, A., Shintaku, M., Li, W.X., Falk, B.W., Dawson, W.O. and Ding, S.W. (2004) Three distinct suppressors of RNA silencing encoded by a 20-kb viral RNA genome. *Proc. Natl Acad. Sci. USA,* **101**, 15742–15747.

Mandadi, K.K. and Scholthof, K.B. (2013) Plant immune responses against viruses: how does a virus cause disease? *Plant Cell,* **25**, 1489–1505.

Meshi, T., Motoyoshi, F., Maeda, T., Yoshiwoka, S., Watanabe, H. and Okada, Y. (1989) Mutations in the *tobacco mosaic virus* 30-kD protein gene overcome Tm-2 resistance in tomato. *Plant Cell,* **1**, 515–522.

Moreno, P., Ambros, S., Albiach-Marti, M.R., Guerri, J. and Pena, L. (2008) *Citrus tristeza virus*: a pathogen that changed the course of the citrus industry. *Mol. Plant Pathol.* **9**, 251–268.

Nwugo, C.C., Doud, M.S., Duan, Y.P. and Lin, H. (2016) Proteomics analysis reveals novel host molecular mechanisms associated with thermotherapy of *'Ca. Liberibacter asiaticus'*-infected citrus plants. *BMC Plant Biol.* **16**, 253–268.

Orbović, V. and Grosser, J.W. (2015). Citrus transformation using juvenile tissue explants. In: *Agrobacterium Protocols, Methods in Molecular Biology* (Wang, K. ed), pp 245–257. New York: Springer.

Ozgur, R., Uzilday, B., Iwata, Y., Koizumi, N. and Turkan, I. (2018) Interplay between the unfolded protein response and reactive oxygen species: a dynamic duo. *J. Exp. Bot.* **69**, 3333–3345.

Podda, A., Simili, M., Del Carratore, R., Mouhaya, W., Morillon, R. and Maserti, B.E. (2014) Expression profiling of two stress-inducible genes encoding for miraculin-like proteins in citrus plants under insect infestation or salinity stress. *J. Plant Physiol.* **171**, 45–54.

Robertson, C.J., Garnsey, S.M., Satyanarayana, T., Folimonova, S.Y. and Dawson, W.O. (2005) Efficient infection of citrus plants with different cloned constructs of *citrus tristeza virus* amplified in *Nicotiana benthamiana* protoplasts. *International Organization of Citrus Virologists Conference Proceedings (1957–2010)* **16**, 187–195.

Ron, D. and Walter, P. (2007) Signal integration in the endoplasmic reticulum unfolded protein response. *Nat. Rev. Mol. Cell Biol.* **8**, 519–529.

Selvakumar, P., Gahloth, D., Tomar, P.P.S., Sharma, N. and Sharma, A.K. (2011) Molecular evolution of miraculin-like proteins in soybean Kunitz super-family. *J. Mol. Evol.* **73**, 369–379.

Sun, Y.D. and Folimonova, S.Y. (2019) The p33 protein of *Citrus tristeza virus* affects viral pathogenicity by modulating a host immune response. *New Phytol.* **221**, 2039–2053.

Taheri, F., Nematzadeh, G., Zamharir, M.G., Nekouei, M.K., Naghavi, M., Mardi, M. and Salekdeh, G.H. (2011) Proteomic analysis of the Mexican lime tree response to "*Candidatus* Phytoplasma aurantifolia" infection. *Mol. BioSyst.* **7**, 3028–3035.

Takai, A., Satoh, M., Matsuyama, T., Ito, A., Nakata, R., Aoyama, T. and Inoue, H. (2013) Secretion of miraculin through the function of a signal peptide conserved in the Kunitz-type soybean trypsin inhibitor family. *FEBS Lett.* **587**, 1767–1772.

Tatineni, S., Robertson, C.J., Garnsey, S.M. and Dawson, W.O. (2011) A plant virus evolved by acquiring multiple nonconserved genes to extend its host range. *Proc. Natl Acad. Sci. USA,* **108**, 17366–17371.

Torres, M.A., Jones, J.D. and Dangl, J.L. (2006) Reactive oxygen species signaling in response to pathogens. *Plant Physiol.* **141**, 373–378.

Wang, M.Y., Zhao, P.M., Cheng, H.Q., Han, L.B., Wu, X.M., Gao, P., Wang, H.Y. *et al*. (2013) The cotton transcription factor TCP14 functions in auxin-mediated epidermal cell differentiation and elongation. *Plant Physiol.* **162**, 1669–1680.

Wang, C., Zhou, M., Zhang, X., Yao, J., Zhang, Y. and Mou, Z. (2017) A lectin receptor kinase as a potential sensor for extracellular nicotinamide adenine dinucleotide in *Arabidopsis thaliana*. *Elife,* **6**, e25474.

Weber, H., Ohnesorge, S., Silber, M.V. and Pfitzner, A.J. (2004) The *Tomato mosaic virus* 30 kDa movement protein interacts differentially with the resistance genes Tm-2 and Tm-2(2). *Adv. Virol.* **149**, 1499–1514.

Xu, Q.F., Cheng, W.S., Li, S.S., Li, W., Zhang, Z.X., Xu, Y.P., Zhou, X.P. *et al*. (2012) Identification of genes required for Cf-dependent hypersensitive cell death by combined proteomic and RNA interfering analyses. *J. Exp. Bot.* **63**, 2421–2435.

Ye, C., Dickman, M.B., Whitham, S.A., Payton, M. and Verchot, J. (2011) The unfolded protein response is triggered by a plant viral movement protein. *Plant Physiol.* **156**, 741–755.

Zhang, L. and Wang, A. (2012) Virus-induced ER stress and the unfolded protein response. *Front. Plant Sci.* **3**, 293.

Zvereva, A.S. and Pooggin, M.M. (2012) Silencing and innate immunity in plant defense against viral and non-viral pathogens. *Viruses,* **4**, 2578–2597.

Supporting information

Additional supporting information may be found online in the Supporting Information section at the end of the article.

Figure S1. The N-terminal portion of the p33 protein lacking the transmembrane domain triggers reactive oxygen species (ROS) burst in *N. benthamiana*.

Figure S2. Multiple sequence alignment of citrus MLP2 sequences.

Figure S3. Generation of p33-overexpressing (OEp33) transgenic *C. macrophylla* lines.

Figure S4. The p33 protein of CTV is restricted in the citrus phloem.

Figure S5. Control set for the CTV-mediated virus-induced gene silencing (VIGS) experiment.

Figure S6. Efficiency of the CTV-based virus-induced gene silencing (VIGS) of citrus *MLP2* in *C. sinensis* (L.) Osbeck plants.

Figure S7. Examination of the virus titres of CTV-GFP and CTV-GFP:Δp33 used for citrus 'bark-flap' inoculation.

Figure S8. Ectopically expressed Cys domain of CmMLP2 forms insoluble granules in *N. benthamiana*.

Figure S9. Effect of the SP, Ktz or Cys domain truncation on the induction of the cellular oxidative stress by the CmMLP2 mutants.

Table S1. The primers used for vector construction and RT-qPCR validation.